



In situ synthesis NiO/F-MWCNTs nanocomposite for adsorption of malachite green dye from polluted water

Salam Hussein Alwan¹ · Hassan Abbas Alshamsi²

Received: 15 January 2022 / Revised: 15 March 2022 / Accepted: 16 March 2022 / Published online: 4 April 2022
© The Author(s), under exclusive licence to Korean Carbon Society 2022

Abstract

The presence of dyes in water is the most popular problem recently, so the current study was directed towards the synthesis of an effective material consisting of NiO and MWCNTs. The NiO/F-MWCNTs nanocomposite was synthesized using a simple hydrothermal method after functionalization of MWCNTs using sulfuric acid and nitric acid and utilized as an efficient surface to adsorption of malachite green dye from polluted water. The nanocomposite sample was characterized using several techniques are X-ray diffraction (XRD), Fourier transform infrared spectroscopy (FTIR), Thermogravimetric analysis (TGA), Field emission scanning electron microscopy (FESEM), High-resolution transmission electron microscopy (HRTEM), Brunauer–Emmett–Teller (BET) surface area analysis, Barrett–Joyner–Halenda (BJH) analysis and Energy dispersive X-ray (EDX). The analytical results showed that the prepared nanocomposite is of good crystalline nature with a particle size of 25.43 nm. A significant specific surface area was 412.08 m²/g which indicates the effective impact of the nanocomposite in the adsorption of malachite green (MG) dye. On the other hand, the effect of adsorbent dose, temperature, acidic function and contact time on the adsorption efficiency of dye was studied. The kinetics of dye adsorption were also investigated employing two kinetic models, pseudo-first-order model and pseudo-second-order model. Finally, the thermodynamic functions were determined to identify the type of the reaction and the spontaneity of the process.

Keywords Functionalized MWCNTs · NiO/F-MWCNTs nanocomposite · Adsorption · Malachite green · Hydrothermal

1 Introduction

Recently, the world started using nanocomposites as an alternative material to improve economic growth in all aspects of life [1]. These composites arise from the interaction of two or more substances with different chemical and physical properties. The most common type of carbon is carbon nanotubes (CNTs) that are used in the fabrication of many composites due to their distinctive properties like chemical stability, great surface area, superb mechanical properties, and good electrical and thermal conductivity [2]. Based on the layers that make up the wall of the carbon tubes, the carbon nanotubes are partitioned into two parts: single-walled carbon nanotubes (SWCNTs) and multi-walled

carbon nanotubes (MWCNTs) [3]. Because of their exceptional properties, both types have played an important role in many industrial, biological and environmental applications such as sensitizers, catalysts, adsorbents, drug carriers, and antibacterial agents. As the functionalization of the MWCNTs surface by oxidation of alcohols utilizing nitric acid and sulfuric acid, this increases the dispersion rate in the reaction solution, in addition to increasing the compatibility with the prepared composites [4]. Therefore, researchers turned towards increasing chemical and thermal stability by doping MWCNTs with several semiconductors such as ZnO, TiO₂, CuO and NiO, as they are considered materials with low economic cost and non-toxic [5]. Nickel oxide (NiO) is a semiconductor material, a cubic structure and has a good bandgap value (3.6–4.0) eV. Nickel oxide exhibits excellent properties such as large surface area, high electronic mobility, good electrical properties, and efficiency at low concentrations [6]. The NiO/F-MWCNTs nanocomposite is an effective material in many medical, biological, industrial and environmental fields because of its low cost and biocompatibility and high adsorption capacity [7]. Due to

✉ Salam Hussein Alwan
salam.hussein@qu.edu.iq

¹ College of Dentistry, University of Al-Qadisiyah, Diwaniya, Iraq

² Department of Chemistry, College of Education, University of Al-Qadisiyah, Diwaniya, Iraq

the promise properties of the nanocomposite, it was applied as an effective substance in the treatment of contaminated water towards dyes and minerals. MWCNTs represent a support substance for the synthesis of nickel oxide nanopowder, preventing their accumulation and making them a hydrophilic surface [8].

The current study included the functionalization of MWCNTs using sulfuric acid and nitric acid and followed by doping with NiO nanoparticles using a simple hydrothermal method. The prepared composite was characterized using several techniques are FTIR, XRD, FESEM, HRTEM, EDX, TGA and BET. Finally, the adsorption efficiency of nanocomposite towards malachite green dye (Fig. 1) from contaminated solutions was studied. The influence of adsorbent dose, acidic function, temperature and equilibrium time on the adsorption process was also investigated (Table 1).

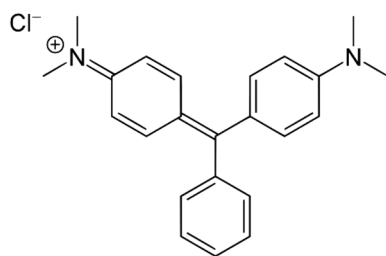


Fig. 1 The structural formula of Malachite Green dye

2 Experimental part

2.1 Chemicals

Pristine-MWCNTs (length $\sim 10\text{--}50\ \mu\text{m}$, diameter $\sim 8\text{--}15\ \text{nm}$) was obtained from Grafton VT (USA). Nitric acid, sulfuric acid and sodium hydroxide were bought from Merck Chemicals. Malachite green (MG [$\text{C}_6\text{H}_5\text{C}(\text{C}_6\text{H}_4\text{N}(\text{CH}_3)_2)_2$]) Cl, M.Wt 364.911 g/mol, purity 90%) was supplied from Chem-supply. Nickel nitrate $\text{Ni}(\text{NO}_3)_2$ was supplied from Sigma-Aldrich (USA). Use deionized water to prepare all solutions.

2.2 Instruments

The crystalline nature of the synthesized nanomaterials was studied using powder X-ray diffraction, XRD-6000 (Shimadzu, Japan) at a scanning rate of $0.03^\circ\ \text{s}^{-1}$ by $\text{Cu K}\alpha$ radiation for diffraction angle (2θ) from 20° to 80° . The oxygen-containing sorts of F-MWCNTs and nanocomposite can be established utilizing FTIR spectroscopy (Nicolet Nexus 670, Shimadzu, Japan) in the region $4000\text{--}400\ \text{cm}^{-1}$ by mixing the samples with KBr discs. The surface morphology of prepared nanomaterials was observed employing field emission scanning electron microscopy FESEM (JEOL, JSM-6701F, voltages 8.0 kV, Japan) and high-resolution transmission electron microscopy HRTEM (Zeiss Libra

Table 1 A list of previous works represents the use of MWCNTs and their composites as adsorbents

CNT	Synthesis Method	Conditions	Applications	References
MWCNTs	Functionalization of MWCNTs	10 ml H_2SO_4 , 30 ml HNO_3 , 10 g MWCNTs, 5 g P_2O_4	Ismate violet 2R dye adsorption	[9]
f-MWNTs	Chemical vapor deposition (CVD)	16 M HNO_3 for 2 h	Golden yellow MR, reactive green HE4BD, congo red dyes adsorption	[10]
Calcium alginate/ MWCNTs	Wet spinning	3 Wt% Sodium alginate, MWCNTs, stirring 30 min and ultrasonic 15 min	Adsorption of methylene blue and methyl orange	[11]
$\text{CoFe}_2\text{O}_4/\text{MWCNT}$	In situ chemical co-precipitation	MWCNTs, $\text{Fe}(\text{NO}_3)_3 \cdot 9\text{H}_2\text{O}$ (1:2), $\text{Co}(\text{NO}_3)_2 \cdot 6\text{H}_2\text{O}$, NaOH (240 g/L)	Methylene blue adsorption	[12]
$\text{Fe}_3\text{O}_4/\text{MWCNTs}$	Chemical co-precipitation	0.01 g $\text{FeCl}_2 \cdot 4\text{H}_2\text{O}$, NaOH (50 ml), 0.0125 g MWCNTs, stirring for 60 min	Methylene blue adsorption	[13]
NiO/MWCNTs	The wet chemical method	MWCNTs, $\text{Ni}(\text{NO}_3)_2 \cdot 6\text{H}_2\text{O}$ in a water/methanol 4/1 v/v and sonicated 2 h		[14]
NiO/CNTs	The direct coprecipitation	3.2 g of $\text{NiCl}_2 \cdot 6\text{H}_2\text{O}$, 50 ml H_2O , 1 g CNT, 1.1 g NaOH and sonicated 10 min	Adsorption of Pb^{2+} ions	[8]
Zn-Ag/ MWCNTs	Double arc discharge	Electric arc discharge system	Methylene blue adsorption	[15]
NiO/F-MWCNTs	Simple hydrothermal method	5 g MWCNTs, 50 ml H_2O , 0.1 M $\text{Ni}(\text{NO}_3)_2$, 1 M NaOH	Malachite green dye adsorption	This work

200 FE, Germany). The thermal stability of nanomaterials was concluded by TGA analysis using a Perkin-Elmer Diamond analyzer in an atmosphere of argon gas at the range of 0–800 °C. The specific surface area and pore size distribution were concluded employing BET and BJH analysis from the adsorption and desorption isotherms using a Quadrasorb SIMP.

2.3 Functionalization of MWCNTs

Covalent functionalization of the MWCNTs was carried out employing the chemical oxidation method. The acid treatment involves the mixing of sulfuric acid (H₂SO₄) and nitric acid (HNO₃) (150/50 ml V/V) with 2 g of MWCNTs. The solution is dispersed at 40 °C for 80 min in the ultrasonic water bath. After dispersion, the suspension is separated utilizing a centrifuge at 10,000 rpm for 15 min. Afterward, the product was washed employing deionized water several times. Then, the material is dried at 60 °C for 18 h in a vacuum oven to obtain the functionalized MWCNTs (F-MWCNTs) [16].

2.4 Synthesis of NiO/F-MWCNTs nanocomposite

The NiO/F-MWCNTs nanocomposite was produced using a simple hydrothermal route. Typically, 3 g of MWCNTs was dispersed in 50 mL of deionized water by sonicator bath for 20 min. After dispersion, the F-MWCNTs solution was mixed with 0.1 M nickel nitrate Ni(NO₃)₂. With a continuous magnetic stirring of the solution, 1 M NaOH solution (35 mL) was added. Finally, the final solution is transferred to the sealed Teflon-lined autoclave (100 mL), closed well and heated at 150 °C for 10 h. After the hydrothermal time is completed, the suspension was cooled down to room temperature for 1 h to obtain the MWCNTs/Ni(OH)₂. The resulting mixture was washed several times with 2-propanol and distilled water. Then, separated using a centrifuge at 10,000 rpm and the sample was collected and dried in a vacuum oven for 60 min. Finally, the powder is calcined at 350 °C for 10 h under aerobic conditions.

2.5 MG adsorption experiments

The adsorption experiments included, prepare the stock solution (20 mg/L) through dissolving 0.02 g MG dye powder into 100 mL distilled water. Then, mixtures of different concentrations in the range 1–20 ppm were prepared and mixing of 10 mL of all solutions with 0.01 g of NiO/F-MWCNTs nanocomposite. The solutions were shaken by placing in a thermostatic digital laboratory water bath (120 rpm) at different times until it reaches the equilibrium time by saturating the surface with dye molecules. After the equilibrium state was reached, the adsorbent particles

were separated using a centrifuge (10,000 rpm) for 10 min. Then, the supernatant solutions were placed in UV–visible spectroscopy to record the dye adsorption at the wavelength of 617 nm. Depending on Eqs. (1 and 2), the quantity of adsorbate (mg/g) and the removal percentage of dye were calculated [17, 18]:

$$q_t = \left(\frac{C_o - C_e}{m} \right) \times V \quad (1)$$

$$R\% = \left(\frac{C_o - C_e}{C_o} \right) \times 100 \quad (2)$$

whereas C_o , C_e represents the initial concentration and the concentration of the dye after adsorption (mg/L), V represents the solution volume (mL) and m represents the adsorbent amount (g).

3 Results and discussion

3.1 Characterization of the synthesized NiO/F-MWCNTs

3.1.1 Fourier transform infrared spectroscopy (FTIR)

FTIR spectroscopy is an effective tool of wide interest in identifying the functional groups in the composition of the nanomaterials. Figure 2 displays the FTIR analysis of F-MWCNTs and NiO/F-MWCNTs nanocomposite in the wavenumber range from 400 to 4000 cm⁻¹. The broad absorption peak at 3427 cm⁻¹ is attributable to the stretching vibration of the hydroxyl groups (-OH). The apparent absorption peaks at 2919 and 2855 cm⁻¹ are attributable to C-H symmetric and asymmetric stretching vibration.

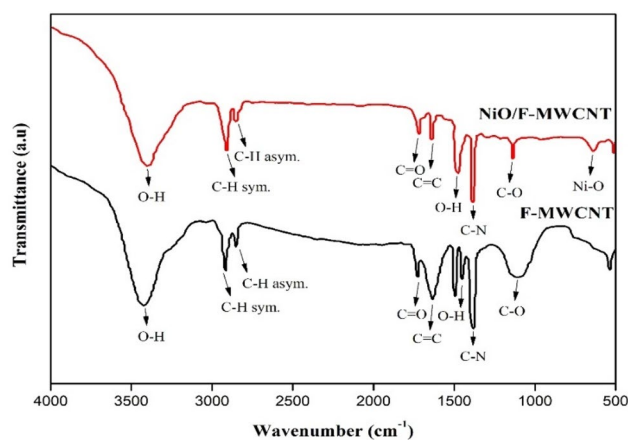


Fig. 2 FTIR spectra of F-MWCNTs and NiO/F-MWCNTs nanocomposite

Also, the absorption peak at 1723 cm^{-1} is attributable to the presence of C=O stretching vibration belonging to the carboxyl groups resulting from the chemical oxidation process [19]. The absorption peak at 1630 cm^{-1} is attributable to C=C stretching vibration in the aromatic rings of the MWCNTs structure. While the absorption peaks appear at 1445 , 1368 , 1110 cm^{-1} owing to the present of the O–H bending, C–N (NO_2), C–O bonds, respectively. After the synthesis of the NiO/F-MWCNTs nanocomposite, a clear decrease in the intensity of the carbonyl top was observed due to the shorthand of the carboxylic sorts (COOH) through the powder thermal treatment. Also, a new absorption peak appears at 626 cm^{-1} due to the vibration of the Ni–O bond. This indicates the success of the nanocomposite synthesis employing the hydrothermal technique [20].

3.1.2 X-rays diffraction (XRD)

Figure 3 illustrates the XRD analysis of F-MWCNTs and NiO/F-MWCNTs nanocomposite in the diffraction angle range $2\theta = 20\text{--}80^\circ$. The X-ray diffractogram of F-MWCNTs exhibits a high-intensity sharp peak at $2\theta = 26.06^\circ$ and a weak peak at $2\theta = 43.25^\circ$ are assigned to the hkl planes of (002) and (100), respectively. Both peaks belong to the hexagonal graphite structure in F-MWCNTs [21]. On the other hand, the XRD pattern of the NiO/F-MWCNTs nanocomposite showed a low-intensity peak at $2\theta = 26.07^\circ$ corresponding to the hkl planes of (002) belong to the F-MWCNTs structure. The observed peaks at $2\theta = 37.59^\circ$, 43.56° , 63.14° , and 75.57° belong to NiO crystal which is assigned to the hkl planes of (111), (200), (220) and (222), respectively [22]. The Debye-Scherrer equation was used to find out the size values of the prepared nanomaterials:

$$D = \frac{0.9\lambda}{\beta \cos \theta} \quad (3)$$

where θ is the Bragg angle, D is crystalline size, β is the full width at half the maximum of the top, λ is the radiation wavelength. It has been found that the crystalline size values for the F-MWCNTs and NiO/F-MWCNTs nanocomposite are 53.33 and 25.43 nm , respectively.

3.1.3 Field emission scanning electron microscopy (FESEM) analysis

FESEM analysis is utilized to reveal the surface morphology which includes the shape, distribution and size of nanoparticles. Figure 4a and b shows FESEM images of F-MWCNTs at two different magnifications. It was observed that short tube shapes (worm-like) with slight defects were observed at the end of the tube. The images showed a decrease in the agglomeration rate of the tubes as a result of surface oxidation due to the present of the carboxylic groups, which reduces the Van der Waals forces linking the tubes [23]. While FESEM images of the NiO/F-MWCNTs nanocomposite in Fig. 4c and d showed heterogeneous spherical shapes representing NiO nanoparticles deposited on the surface of tangled tubes representing F-MWCNTs. It was observed that the distribution of NiO nanoparticles is irregular on the F-MWCNTs surface. The results show the successful attachment of NiO with F-MWCNTs using the hydrothermal method [24]. Finally, it was found that the particle size of the F-MWCNTs and NiO/F-MWCNTs nanocomposite are 37.26 and 33.14 nm , respectively. The observed sizes are almost agreed with the results of the XRD analysis.

3.1.4 Energy-dispersive X-ray spectroscopy (EDX)

EDX spectroscopy is a very popular technique utilized to recognize the primary compositions of synthesized solid nanomaterials. Figure 5 demonstrates the EDX analysis of F-MWCNTs and NiO/F-MWCNTs nanocomposite. EDX analysis of F-MWCNTs showed the presence of carbon and oxygen in weight ratios 82.81% and 18.18% , respectively. This indicates the success of the process of adding carboxylic groups to the MWCNTs surface. In addition, the absence of any additional peaks confirms the purity of the prepared MWCNTs sample. While the EDX of NiO/F-MWCNTs nanocomposite showed the existence of oxygen, nickel and carbon in weight ratios of 48.77% , 37.79% and 13.44% , respectively. This confirms the success of the decoration of the F-MWCNTs surface by NiO nanoparticles using the hydrothermal method.

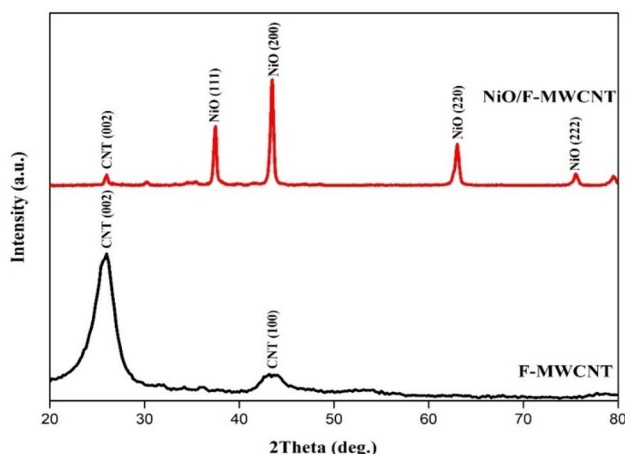


Fig. 3 XRD patterns of F-MWCNTs and NiO/F-MWCNTs nanocomposite

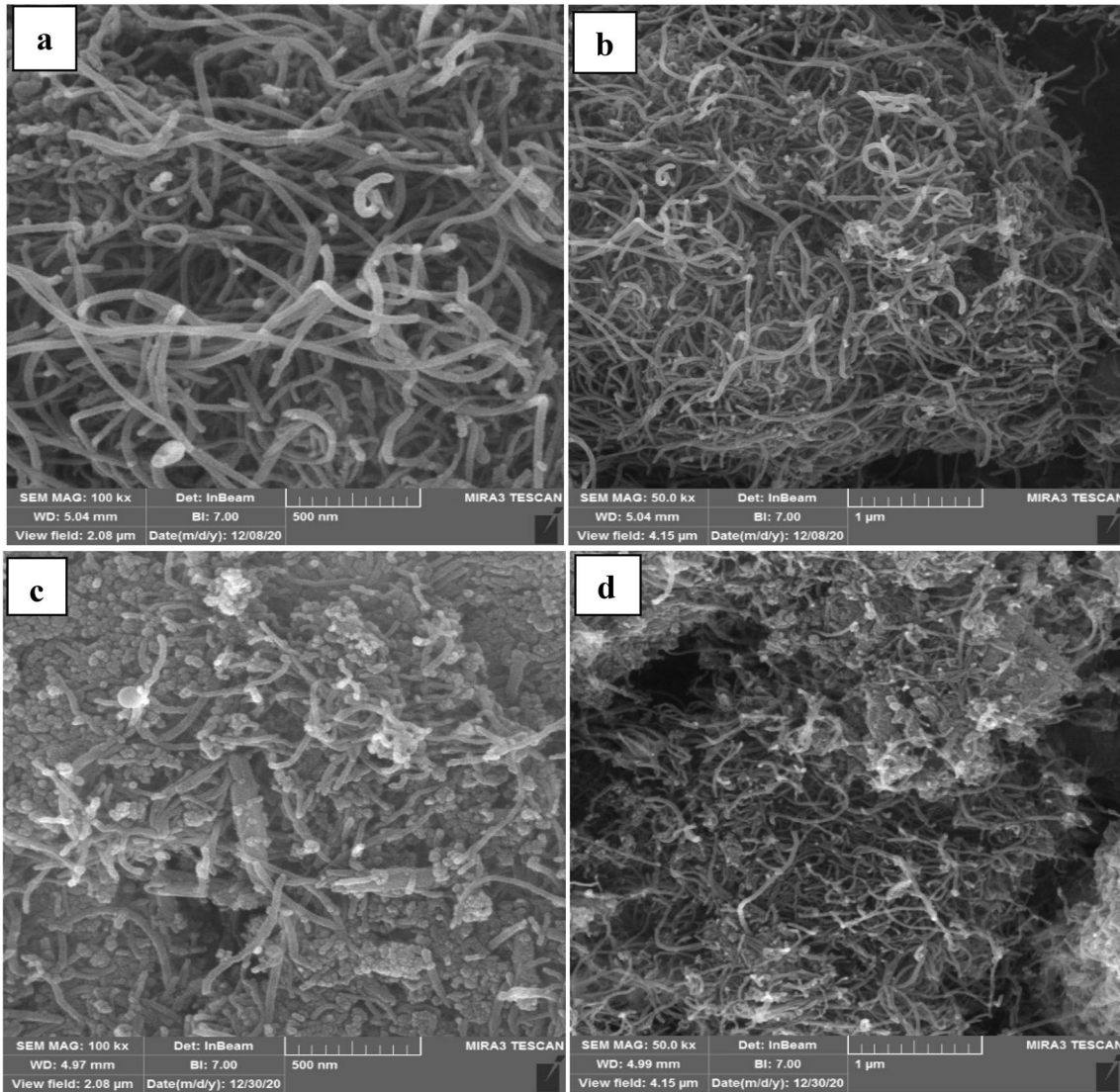


Fig. 4 FESEM image **a, b** F-MWCNTs and **c, d** NiO/F-MWCNTs nanocomposite

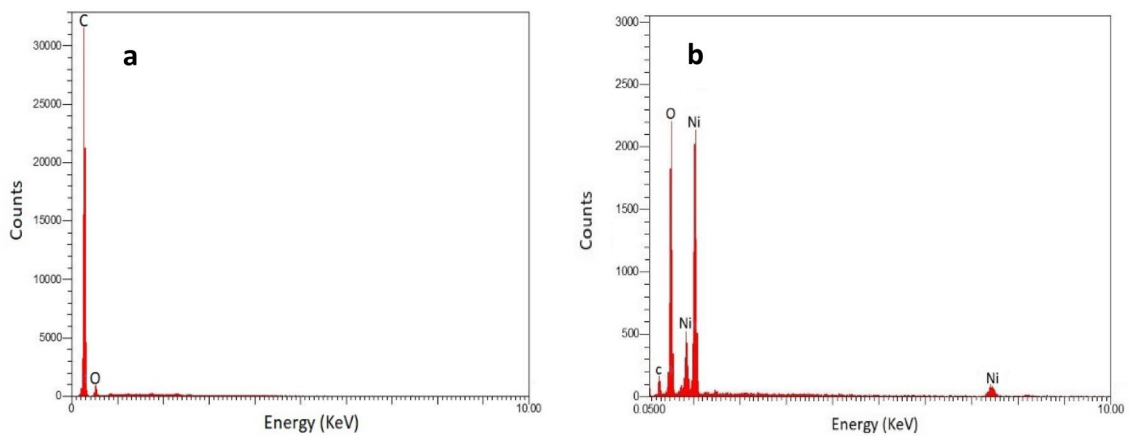


Fig. 5 EDX spectra of **a** F-MWCNTs and **b** NiO/F-MWCNTs nanocomposite

3.1.5 High-resolution transmission electron microscopy (HRTEM) analysis

HRTEM is a common technique for identifying the morphology, structural details, particle size and crystalline defects of nanomaterials on the atomic scale [25]. Figure 6a HRTEM image of MWCNTs shows the presence of a cylindrical tube with regular edges and has an average diameter of 33.5 nm. Figure 6b HRTEM image of NiO/F-MWCNTs nanocomposite shows the presence of heterogeneous spherical shapes distributed on the surface of the nanotubes with a significant decrease in the accumulation rate of nanoparticles with an average diameter of up to 45.14 nm. This morphology is consistent with a previous report [26].

3.1.6 Specific surface area and pore volume estimate

The BET is a widely used method for estimating the specific surface area (SSA) depending on the N_2 gas adsorption–desorption measurements at 77 K. While the BJH method was utilized to identify the specific pore volume distribution of the solid surfaces. The BET data exhibited that the surface area value of F-MWCNTs is $332.12 \text{ m}^2/\text{g}$, while the BJH data revealed that the pore volume value is $0.16 \text{ cm}^3/\text{g}$. It was noticed that the adsorption isotherm of F-MWCNTs follows the type II isotherm, which confirms that the physical adsorption is obtained on porous surfaces through a monolayer covering, followed by a multilayer covering (Fig. 7). On the other hand, it was found that the specific surface area and the pore volume of the NiO/F-MWCNTs nanocomposite are $412.08 \text{ m}^2/\text{g}$ and $0.13 \text{ cm}^3/\text{g}$, respectively. In addition, the nanocomposite isotherm follows type IV,

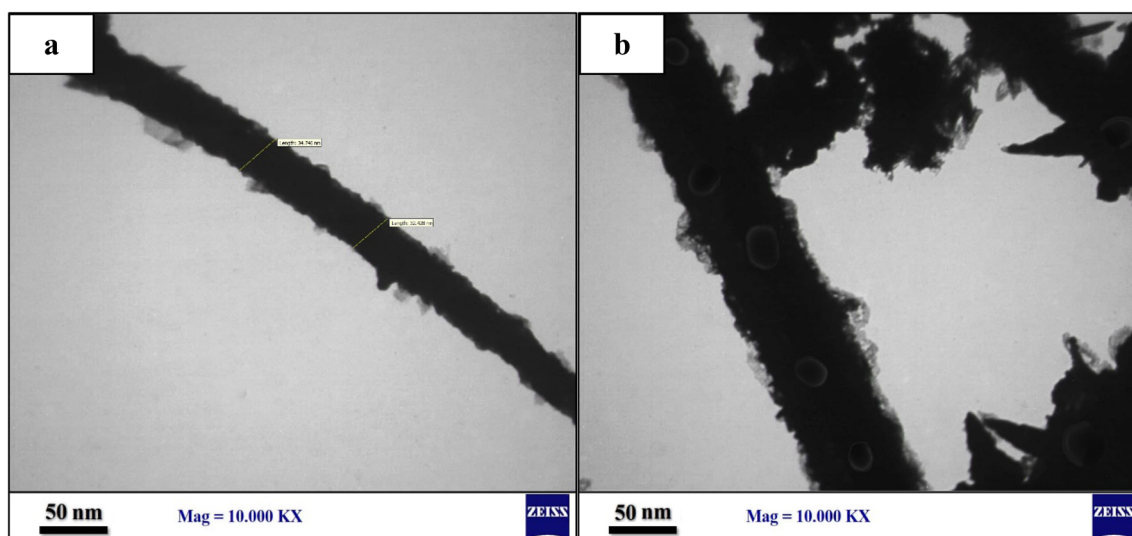


Fig. 6 HRTEM image a F-MWCNTs and b NiO/F-MWCNTs nanocomposite

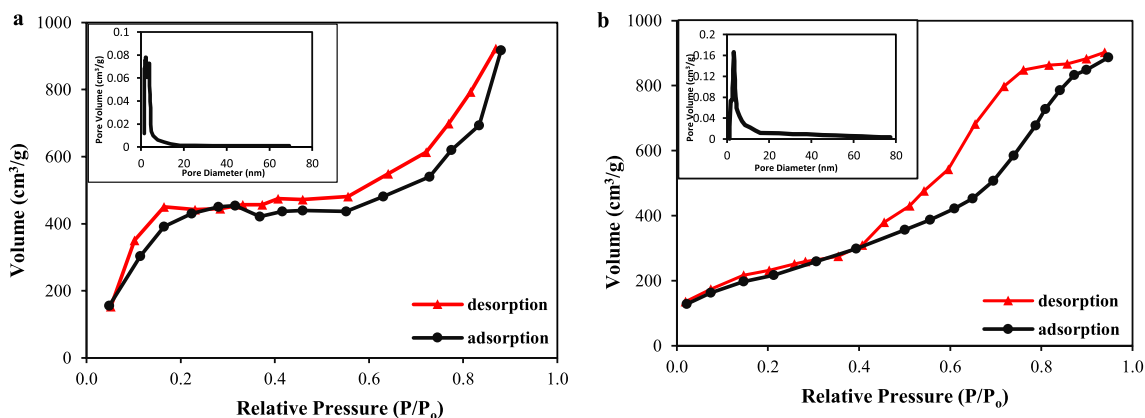


Fig. 7 Nitrogen adsorption and desorption isotherms and BJH plot (insert figure) of the a F-MWCNTs and b NiO/F-MWCNTs nanocomposite

and this indicates that the sample is of a mesoporosity nature. The BJH results showed that the pore diameter of the F-MWCNTs and NiO/F-MWCNTs nanocomposite are 2.4 and 2.6 nm, respectively (insert Fig. 7). The obtained pore diameter values refer to the mesoporous composition of both surfaces [27].

3.1.7 Thermogravimetric analysis (TGA)

The TGA analysis is a quick and facile way to determine the thermal stability of prepared nanomaterials as a result of changing their properties through losing weight with increasing temperature. Figure 8 shows TGA analysis of F-MWCNTs and NiO/F-MWCNTs nanocomposite in the range of 0–800 °C. The F-MWCNTs showed low thermal stability, resulting in a weight loss up to 99.58% in the range of 200–580 °C owing to the water elimination, functional groups and consequently the thermal decomposition of other molecules with the oxidation of carbon [21]. After decorating F-MWCNTs with NiO nanoparticles, the thermal stability is significantly increased due to the low rate of mass loss 28.32% in the range 400–520 °C is owing to the rapid pyrolysis of the residual oxygen types. In addition to the evaporation of CO₂ and CO gases. The obtained thermal data confirmed that the thermal stability of the NiO/F-MWCNTs nanocomposite is higher than F-MWCNTs [28].

3.2 Investigation of MG adsorption

3.2.1 Influence of the F-MWCNTs and NiO/F-MWCNTs nanocomposite mass

The influence of F-MWCNTs and NiO/F-MWCNTs doses at different masses (0.04–0.28 g) towards adsorption of malachite green dye was studied. Figure 9 shows the increase in

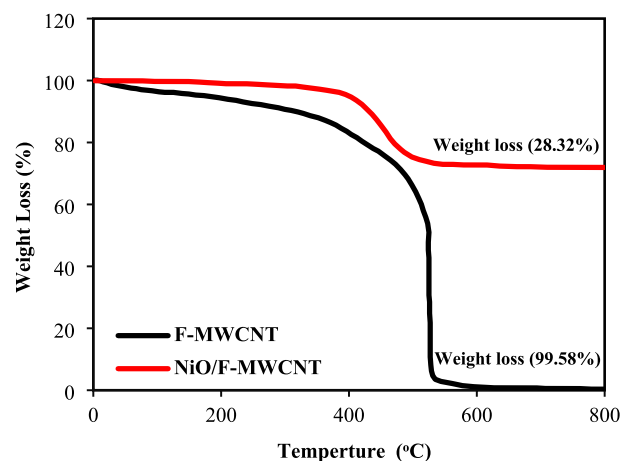


Fig. 8 TGA thermograms of F-MWCNTs and NiO/F-MWCNTs nanocomposite

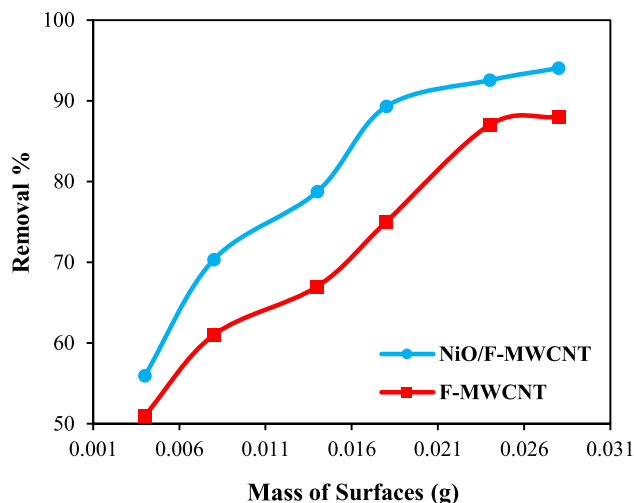


Fig. 9 Influence of adsorbents mass on the adsorption of MG dye

the dye removal percentage with the increase in the mass of both surfaces. The NiO/F-MWCNTs nanocomposite showed a dye removal efficiency of up to 94% which is higher than the removal efficiency of F-MWCNTs (up to 88%). Therefore, all subsequent experiments were performed with NiO/F-MWCNTs.

3.2.2 Influence of contact time

The influence of contact time on the adsorption capacity of malachite green dye on NiO/F-MWCNTs nanocomposite with different times (1–140 min) at the temperature of 25 °C and initial dye concentration 10 ppm was studied. Figure 10 shows that increasing the adsorption contact time beside an increase in the adsorption capacity up to time 140 min when removal

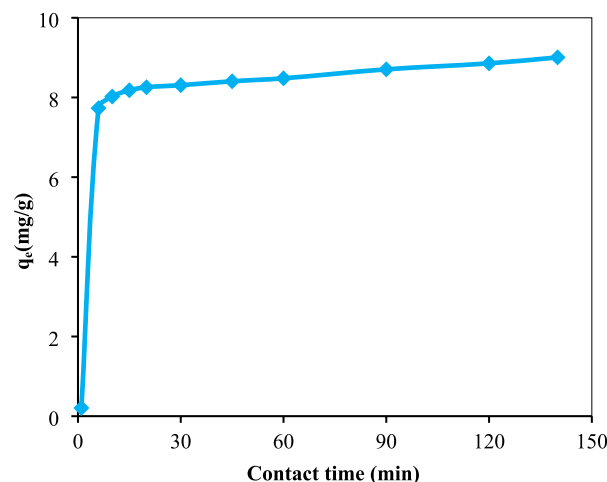


Fig. 10 Influence of contact time on the adsorption of MG dye

efficiency of 90.06%. After that, the adsorption became almost constant due to the saturation of the active sites with dye molecules [29].

3.2.3 Adsorption kinetics evaluation

In this section, the interaction between the MG dye and the NiO/F-MWCNTs nanocomposite and their kinetics were identified. Two kinetic models are pseudo-first-order and pseudo-second-order models, have been studied. Equation 4 shows the pseudo-first-order model [30]:

$$\ln(q_e - q_t) = \ln q_e - k_1 t \quad (4)$$

where k_1 is the pseudo-first-order adsorption rate constant (min^{-1}), q_e and q_t are equilibrium adsorption capacity (mg g^{-1}) and the adsorption capacity at a certain time (mg g^{-1}). Finally, the values of the pseudo-first-order constant and equilibrium adsorption capacity can be estimated from the linear relationship between $\ln(q_e - q_t)$ and time, since the k_1 represents the slope and the q_e represents the intercept. Equation 5 shows the pseudo-second-order model [31]:

$$\frac{t}{q_t} = \frac{1}{k_2 q_e^2} + \left(\frac{1}{q_t}\right)t \quad (5)$$

where k_2 is the pseudo-second-order adsorption rate constant ($\text{g mg}^{-1} \text{min}^{-1}$). The linear relationship between t/q_t with time can calculate the values of the equilibrium adsorption capacity (slope) and the k_2 (intercept). The kinetic constants and correlation coefficients for both models were calculated in Table 2. It was noted that the correlation coefficient for the pseudo-first-order model is $R^2=0.214$, and this confirms the incompatibility of the model with the adsorption process between the dye and the NiO/F-MWCNTs nanocomposite. Figure 11 displays the linearity of the second-order model is $R^2=0.935$, and this indicates that the interaction between adsorbate and adsorbent follows the pseudo-second-order model. The pseudo-second-order model suggests that the higher number of unoccupied active sites, the higher the adsorption rate. In addition, covering the adsorbent surface does not change the reaction energy [31].

3.2.4 Influence of temperature and adsorption thermodynamics

The influence of temperature on the adsorption process was investigated using various temperatures 10, 20 and 30 °C.

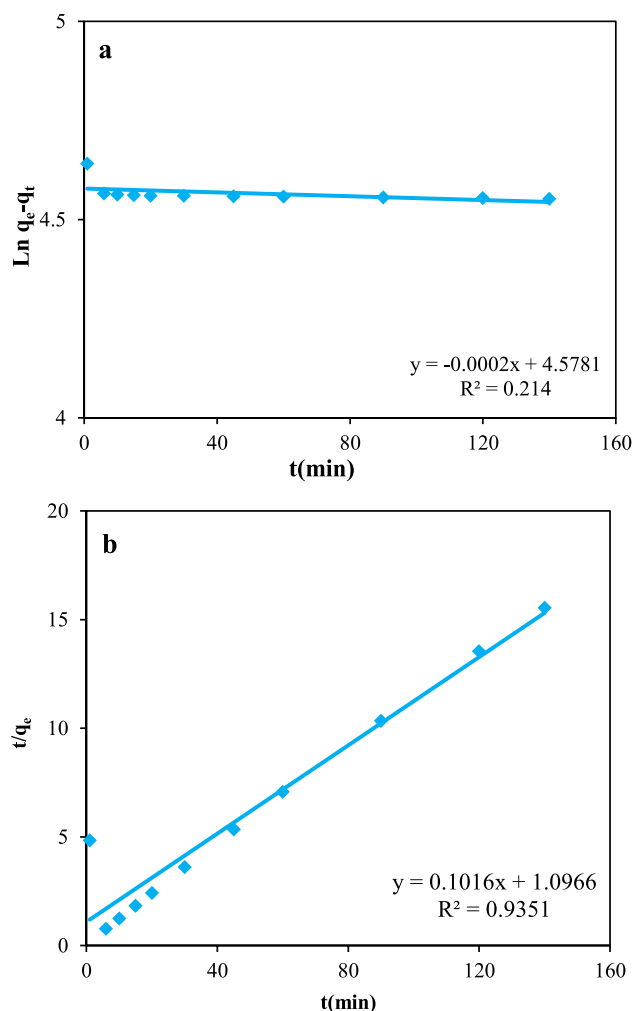


Fig. 11 a Pseudo first-order and b pseudo-second-order kinetic models for MG dye adsorption

Figure 12 shows the gradual increase in the adsorption capacity with rising solution temperature, this indicates an increase in the spread of cations of the malachite green dye on the active sites of the prepared nanocomposite surface owing to the increase in kinetic energy. The thermodynamic parameters that have been studied include Gibbs free energy (ΔG°), enthalpy change (ΔH°) and change in entropy (ΔS°) whose equations are mentioned below:

$$\Delta G^\circ = -RT \ln K_a \quad (6)$$

Table 2 Kinetics parameters for MG dye adsorption on NiO/F-MWCNTs

Dye	Pseudo-first order			Pseudo-second order			
	k_1	q_e	R^2	k_2	q_e	h	R^2
MG	0.0002	97.32	0.214	0.0096	1.842	0.9347	0.935

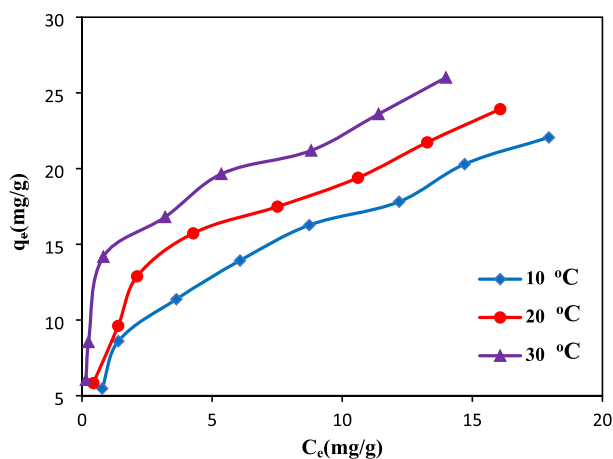


Fig. 12 Influence of the temperature on the MG dye adsorption

$$\Delta G^\circ = \Delta H^\circ - T\Delta S^\circ \tag{7}$$

$$\Delta S^\circ = \frac{\Delta H^\circ - \Delta G^\circ}{T} \tag{8}$$

where R represents the universal gas constant (8.314 J/mol K), K_a represents adsorption equilibrium constant and T represents the temperature (K). Depending on the Van't Hoff Eq. (9), $\ln K_a$ versus T^{-1} is plotted to estimate the ΔH° value from the slope and the ΔS° value from an intercept. The mathematical expression of the Vant Hoff equation is as shown below [32]:

$$\ln K_a = \frac{\Delta S^\circ}{R} - \frac{\Delta H^\circ}{RT} \tag{9}$$

The results obtained from the thermodynamic calculations showed that the treatment process has a negative Gibbs free energy ($\Delta G^\circ = -1.363$), meaning that the interaction between the nanocomposite and the dye occurs spontaneously. Moreover, the enthalpy change value is positive ($\Delta H^\circ = +12.31$) and this suggests that the adsorption is endothermic. On the other hand, the change in entropy showed a positive value ($\Delta S^\circ = +46.69$), which indicates a high rate of randomness during the adsorption process [33].

3.2.5 Adsorption isotherms

The adsorption isotherm represents the relationship between the quantity of adsorbate (q_e) and the equilibrium concentration at a constant temperature [34]. Three types of adsorption isotherms have been studied, they are Langmuir, Freundlich and Temkin models. Langmuir adsorption isotherm suggests that the reaction system between the adsorbate and the adsorbent is monolayered, homogeneous and all active adsorption sites have equal activation energy. Equation 10 represents the mathematical form of the Langmuir model [35]:

$$\frac{C_e}{q_e} = \frac{C_e}{q_m} + \frac{1}{K_L q_m} \tag{10}$$

where C_e represents the equilibrium concentration of MG dye (mg L^{-1}), q_m and q_e represents the maximum adsorption capacity and the adsorption capacity at equilibrium (mg g^{-1}), respectively. Freundlich adsorption isotherm describes the reversible, heterogeneous and multilayer adsorption, especially on the active carbon materials or organic compounds [36]. The mathematical expression of the Freundlich model is shown in Eq. (11):

$$\log q_e = \log K_f + \frac{1}{n} \log C_e \tag{11}$$

where K_f represents the adsorption constant of the Freundlich model, n represents the linear factor. Temkin adsorption isotherm suggests that the reaction temperature for all active species decreases linearly with surface coverage. Equation 12 shows the linear form of the Temkin model [37]:

$$q_e = B \ln K_T + B \ln C_e \tag{12}$$

where K_T represents the adsorption constant of the Temkin model. Table 3 and Fig. 13 display the correlation coefficients for the three models and the adsorption isotherms data. It was found that the correlation coefficients of Langmuir and Temkin isotherms are $R^2 = 0.5014$ and 0.879 , respectively. A lower value of the R^2 indicates that both isotherms are not suitable for the adsorption process. In contrast, the value of the correlation coefficient of the Freundlich isotherm model is $R^2 = 0.99$, which indicates that the isotherm fits the obtained adsorption data. We conclude from this that the adsorption reaction is heterogeneous and multilayered.

Table 3 Langmuir, Freundlich and Temkin isotherm constants

Langmuir			Freundlich			Temkin		
K_L	q_m	R^2	K_F	n	R^2	K_T	B	R^2
0.017	400	0.5014	7.284	1.101	0.990	7.739	0.032	0.879

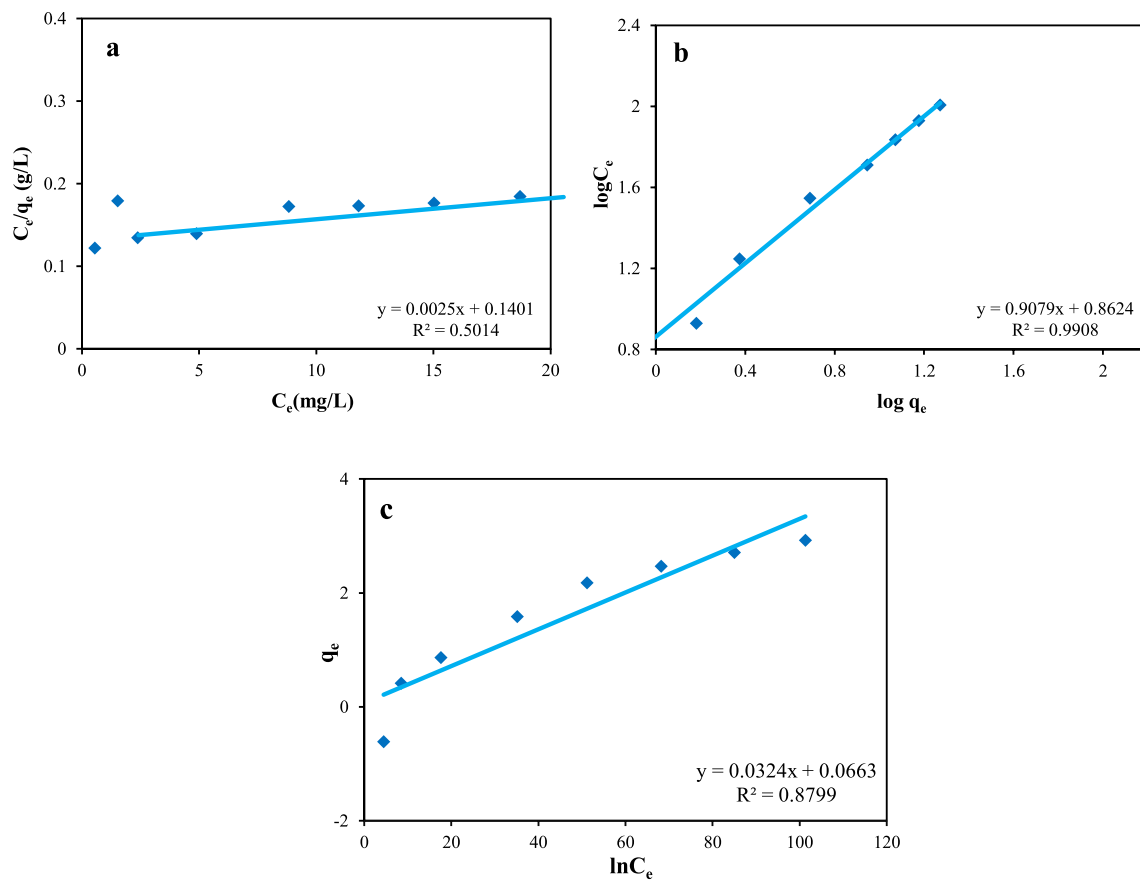


Fig. 13 Adsorption isotherms **a** Langmuir model, **b** Freundlich model and **c** Temkin model

3.2.6 Influence of solution pH

The influence of the pH in the range of 2–12 was studied as an influencing factor on the adsorption nature through changing surface charges according to the pH medium. Figure 14a displays the relationship between the amount

of adsorbate and the acidic function. It can be seen that at low pH values, decreases in the removal percentage of the MG dye on the NiO/F-MWCNTs nanocomposite due to the ability of hydrogen ions to attach with the active surface sites which is faster than the dye molecules. At high pH values, increases of the adsorption efficiency owing to

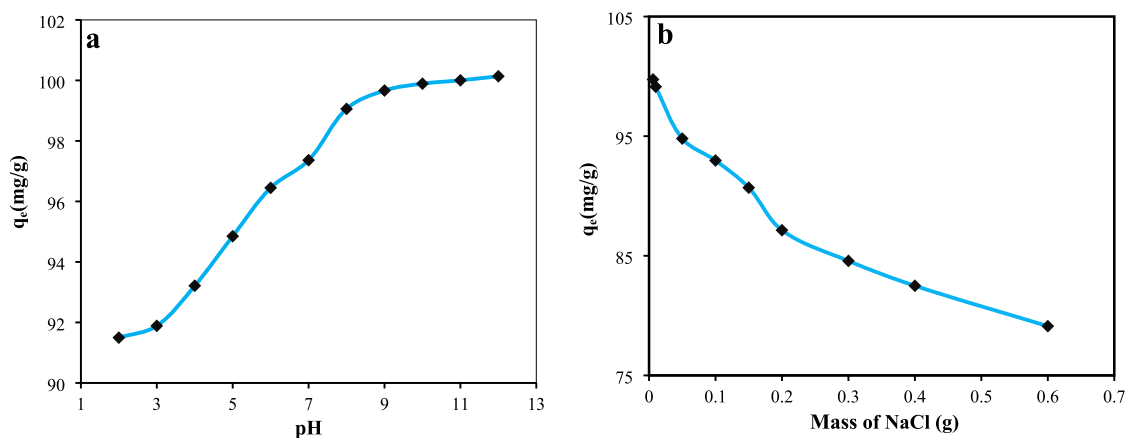


Fig. 14 Influence of **a** pH medium and **b** NaCl weight on MG dye adsorption

the increase of negative electrical charges (OH^-) on the nanocomposite surface, and thus increases the electrostatic interaction between the positively charged MG molecules with the negatively charged adsorbent [38].

3.2.7 Influence of salt concentration

The presence of inorganic salts in the reaction solution is a significant index that changes the removal efficiency and affects the surface charge. Figure 14b displays the influence of NaCl mass on the amount of MG adsorbed by the NiO/F-MWCNTs nanocomposite. It was noticed that an increase in NaCl mass decreased adsorption capacity. This behavior is due to the competition between positively charged MG molecules and the sodium ions (Na^+) to occupying the same negatively charged active sites on the NiO/F-MWCNTs surface [39]. Similar was behaviors in aqueous solution previously studied by Runping et al. [40].

4 Conclusions

In the current study, the NiO/F-MWCNTs nanocomposite was fabricated via a hydrothermal process. It was found that the synthesized nanocomposite has good properties of particle size is 25 nm, a good large surface area and high thermal stability, and this makes it an absorbent and effective material in removing hazardous substances from polluted water. It was observed that the removal efficiency of the malachite green dye on the nanocomposite was up to 94%. Most of the factors affecting the adsorption process like surfaces mass, temperature, pH, salt concentration and contact time are studied. It was found that the removal efficiency increases besides increasing the surface's mass, the temperature and the acidic function. While adsorption kinetics models were applied, namely the pseudo-first-order model and the pseudo-second-order model, as it was established that the reaction between dye and nanocomposite obeys the pseudo-second-order model. Calculations of thermodynamic functions (ΔH° , ΔG° , ΔS°) showed that the adsorption reaction is endothermic, spontaneous and highly random. In contrast, the results of the adsorption isotherms displayed that the reaction between adsorbate and adsorbent obeys the Freundlich isotherm model ($R^2 = 0.990$) and does not agree with the Langmuir and Temkin isotherm model. This indicates that the adsorption is heterogeneous and multilayered. Finally, the removal ability decreases with the increase in the amount of inorganic salt added to the adsorption solution.

Declarations

Conflict of interest The authors declare that there are no conflicts of interest regarding the publication of this manuscript.

References

- Petronella F, Truppi A, Ingrosso C, Placido T, Striccoli M, Curri ML, Comparelli R (2017) Nanocomposite materials for photocatalytic degradation of pollutants. *Catal Today* 281:85–100
- Sajid MI, Jamshaid U, Jamshaid T, Zafar N, Fessi H, Elaissari A (2016) Carbon nanotubes from synthesis to in vivo biomedical applications. *Int J Pharm* 501(1–2):278–299
- Pandey P, Dahiya M (2016) Carbon nanotubes: types, methods of preparation and applications. *Carbon* 1:4
- Yao X, Kou X, Qiu J (2016) Multi-walled carbon nanotubes/polyaniline composites with negative permittivity and negative permeability. *Carbon* 107:261–267
- Belin T, Epron F (2005) Characterization methods of carbon nanotubes: a review. *Mater Sci Eng B* 119(2):105–118
- Khoshhesab ZM, Sarfaraz M (2010) Preparation and characterization of NiO nanoparticles by chemical precipitation method. *Synth React Inorg Met-Org Nano-Met Chem* 40(9):700–703
- Yu W, Li B, Ding SJ (2016) Electroless fabrication and supercapacitor performance of CNT@ NiO-nanosheet composite nanotubes. *Nanotechnology* 27(7):075605
- Divya TN, Zare K, Taleshi F, Yousefi M (2017) Synthesis, characterization, and application of nickel oxide/CNT nanocomposites to remove Pb^{2+} from aqueous solution. *J Nanostruct Chem* 7(3):273–281
- Abualnaja KM, Alprol AE, Ashour M, Mansour AT (2021) Influencing multi-walled carbon nanotubes for the removal of ismarte violet 2R dye from wastewater: isotherm, kinetics, and thermodynamic studies. *Appl Sci* 11(11):4786
- Mishra AK, Arockiadoss T, Ramaprabhu S (2010) Study of removal of azo dye by functionalized multi walled carbon nanotubes. *Chem Eng J* 162(3):1026–1034
- Sui K, Li Y, Liu R, Zhang Y, Zhao X, Liang H, Xia Y (2012) Biocomposite fiber of calcium alginate/multi-walled carbon nanotubes with enhanced adsorption properties for ionic dyes. *Carbohydr Polym* 90(1):399–406
- Farghali AA, Bahgat M, El Roubi WMA, Khedr MH (2012) Decoration of MWCNTs with CoFe_2O_4 nanoparticles for methylene blue dye adsorption. *J Solut Chem* 41(12):2209–2225
- Suwattanamala A, Bandis N, Tedsree K, Issro C (2017) Synthesis, characterization and adsorption properties of $\text{Fe}_3\text{O}_4/\text{MWCNT}$ magnetic nanocomposites. *Mater Today* 4(5):6567–6575
- Sahebians S, Zebarjad SM, Khaki JV, Lazzeri A (2016) The decoration of multi-walled carbon nanotubes with nickel oxide nanoparticles using chemical method. *Int Nano Lett* 6(3):183–190
- Aljohani FS, Elsafi M, Ghoneim NI, Toderas M, Sayyed MI, Mohafez H, El-Khatib M (2021) Water treatment from MB using Zn-Ag MWCNT synthesized by double arc discharge. *Materials* 14(23):7205
- Likodimos V, Steriotis TA, Papageorgiou SK, Romanos GE, Marques RR, Rocha RP, Falaras P (2014) Controlled surface functionalization of multiwall carbon nanotubes by HNO_3 hydrothermal oxidation. *Carbon* 69:311–326
- Altaa SH, Alshamsi HA, Al-Hayder LS (2018) Synthesis and characterization of rGO/ Co_3O_4 composite as nanoadsorbent for rhodamine 6G dye removal. *Desalin Water Treat* 114:320–331
- Hussain N, Alwan S, Alshamsi H, Sahib IJ (2020) Green synthesis of S-and N-codoped carbon nanospheres and application

- as adsorbent of Pb (II) from aqueous solution. *Int J Chem Eng.* <https://doi.org/10.1155/2020/9068358>
19. Her SC, Lai C (2013) Dynamic behavior of nanocomposites reinforced with multi-walled carbon nanotubes (MWCNTs). *Materials* 6(6):2274–2284
 20. López E, Kim J, Shanmugaraj AM, Ryu SH (2012) Multiwalled carbon nanotubes-supported Nickel catalysts for the steam reforming of propane. *J Mater Sci* 47(6):2985–2994
 21. Arunkumar T, Karthikeyan R, Ram Subramani R, Viswanathan K, Anish M (2020) Synthesis and characterisation of multi-walled carbon nanotubes (MWCNTs). *Int J Ambient Energy* 41(4):452–456
 22. Yuan C, Xiong S, Zhang X, Shen L, Zhang F, Gao B, Su L (2009) Template-free synthesis of ordered mesoporous NiO/poly (sodium-4-styrene sulfonate) functionalized carbon nanotubes composite for electrochemical capacitors. *Nano Res* 2(9):722–732
 23. Zaman A, Rashid TU, Khan MA, Rahman MM (2015) Preparation and characterization of multiwall carbon nanotube (MWCNT) reinforced chitosan nanocomposites: effect of gamma radiation. *BioNanoScience* 5(1):31–38
 24. Fayemi OE, Adekunle AS, Ebenso EE (2017) Electrochemical determination of serotonin in urine samples based on metal oxide nanoparticles/MWCNT on modified glassy carbon electrode. *Sens Bio-Sens Res* 13:17–27
 25. Lone IH, Aslam J, Akhter A (2021) Characterization of advanced green materials. *Advanced green materials*. Elsevier, Amsterdam, pp 31–41
 26. Shaikshavali P, Reddy TM, Gopal TV, Venkataprasad G, Kotakadi VS, Palakollu VN, Karpoornath R (2020) A simple sonochemical assisted synthesis of nanocomposite (ZnO/MWCNTs) for electrochemical sensing of Epinephrine in human serum and pharmaceutical formulation. *Colloids Surf A* 584:124038
 27. Li G, Li Y, Chen J, Zhao P, Li D, Dong Y, Zhang L (2017) Synthesis and research of egg shell-yolk NiO/C porous composites as lithium-ion battery anode material. *Electrochim Acta* 245:941–948
 28. Luo Y, Wang K, Luo S, Zhao F, Wu H, Jiang K, Wang J (2018) Three-dimensional carbon nanotube/transition-metal oxide sponges as composite electrodes with enhanced electrochemical performance. *ACS Appl Nano Mater* 1(6):2997–3005
 29. Gil A, Santamaría L, Korili SA (2018) Removal of caffeine and diclofenac from aqueous solution by adsorption on multiwalled carbon nanotubes. *Colloid Interface Sci Commun* 22:25–28
 30. Özcan A, Özcan AS (2005) Adsorption of acid red 57 from aqueous solutions onto surfactant-modified sepiolite. *J Hazard Mater* 125(1–3):252–259
 31. Olgun A, Atar N (2009) Equilibrium and kinetic adsorption study of Basic Yellow 28 and Basic Red 46 by a boron industry waste. *J Hazard Mater* 161(1):148–156
 32. Lima EC, Gomes AA, Tran HN (2020) Comparison of the non-linear and linear forms of the van't Hoff equation for calculation of adsorption thermodynamic parameters (ΔS° and ΔH°). *J Mol Liq* 311:113315
 33. Jiang C, Wang X, Qin D, Da W, Hou B, Hao C, Wu J (2019) Construction of magnetic lignin-based adsorbent and its adsorption properties for dyes. *J Hazard Mater* 369:50–61
 34. Al-Ghouti MA, Da'ana DA (2020) Guidelines for the use and interpretation of adsorption isotherm models: a review. *J Hazard Mater* 393:122383
 35. Rajahmundry GK, Garlapati C, Kumar PS, Alwi RS, Vo DVN (2021) Statistical analysis of adsorption isotherm models and its appropriate selection. *Chemosphere* 276:130176
 36. Ragadhita RISTI, Nandiyanto ABD, Nugraha WC, Mudzakhir AHMAD (2019) Adsorption isotherm of mesopore-free submicron silica particles from rice husk. *J Eng Sci Technol* 14(4):2052–2062
 37. Balarak D, Mostafapour FK, Azarpira H, Joghataei A (2017) Langmuir, Freundlich, Temkin and Dubinin–radushkevich isotherms studies of equilibrium sorption of ampicillin onto montmorillonite nanoparticles. *J Pharm Res Int.* <https://doi.org/10.9734/JPRI/2017/38056>
 38. Alshameri A, He H, Zhu J, Xi Y, Zhu R, Ma L, Tao Q (2018) Adsorption of ammonium by different natural clay minerals: characterization, kinetics and adsorption isotherms. *Appl Clay Sci* 159:83–93
 39. Oloo CM, Onyari JM, Wanyonyi WC, Wabomba JN, Muinde VM (2020) Adsorptive removal of hazardous crystal violet dye from aqueous solution using *Rhizophora mucronata* stem-barks: Equilibrium and kinetics studies. *Environ Chem Ecotoxicol* 2:64–72
 40. Han R, Zhang J, Han P, Wang Y, Zhao Z, Tang M (2009) Study of equilibrium, kinetic and thermodynamic parameters about methylene blue adsorption onto natural zeolite. *Chem Eng J* 145(3):496–504

Publisher's Note Springer Nature remains neutral with regard to jurisdictional claims in published maps and institutional affiliations.